Journal of Zhejiang University-SCIENCE B (Biomedicine & Biotechnology)
ISSN 1673-1581 (Print); ISSN 1862-1783 (Online)
www.zju.edu.cn/jzus; www.springerlink.com
E-mail: jzus@zju.edu.cn

Clodronate-superparamagnetic iron oxide-containing liposomes attenuate renal injury in rats with severe acute pancreatitis*

Sheng-chun DANG†, Yan-hua ZENG, Ping-jiang WANG, Bao-ding CHEN, Rong-fang CHEN, Arun KUMAR SINGH, Pankaj KUMAR, Shu FENG, Lei CUI, Hao WANG, Jian-xin ZHANG†‡

(*Department of General Surgery, the Affiliated Hospital of Jiangsu University, Zhenjiang 212001, China*)

†E-mail: dscgu@163.com; zhangjx@ujs.edu.cn

Received Sept. 10, 2013; Revision accepted Nov. 11, 2013; Crosschecked May 20, 2014

Abstract: Background and objective: It has been shown that macrophages play an important role in the development of severe acute pancreatitis (SAP), and eventually lead to multiple organ failure (MOF). Clodronate-liposome selectively depleted macrophages. This study was to investigate the role of renal macrophage infiltration in acute renal injury in rats with SAP and to evaluate the potential of superparamagnetic iron oxide (SPIO)-enhanced magnetic resonance imaging (MRI) for diagnosis. Methods: Superparamagnetic Fe_3O_4 nanoparticles were prepared by chemical coprecipitation. SPIO-liposomes and SPIO-clodronate-liposomes were prepared by the thin film method. SAP models were prepared by injection of sodium taurocholate into the subcapsular space of rat pancreas. Sprague-Dawley rats were randomly divided into a control group, SAP plus SPIO-liposome (P) group, and SAP plus SPIO-clodronate-containing liposome (T) group. Kidney injury was evaluated by T2-weighted MRI scan. The levels of serum amylase (SAM), blood urea nitrogen (BUN), and serum creatinine (SCr) were measured by an automated enzymatic method. Serum tumor necrosis factor-α (TNF-α) was measured by enzyme-linked immunosorbent assay (ELISA). Pathological changes in the pancreas and kidney were observed using hematoxylin and eosin (H&E) staining, while cell apoptosis was detected with terminal deoxynucleotidyl transferase dUTP nick end labeling (TUNEL) staining. In addition, the macrophage markers (CD68) of the renal tissue were detected with immunohistochemistry. Results: The pathological changes in the pancreas and kidneys of rats in the T group were milder than those in the P group. The MRI signal intensity of the kidneys in the P and T groups was significantly lower than that in the control group. There were significant changes in the two experimental groups (P<0.01). The levels of SAM, Bun, SCr, and TNF-α in rats in the P group were higher than those in the control group (P<0.01) and in the T group (P<0.01). The apoptosis of the kidney in the T group was higher than that in the P group at 2 and 6 h (P<0.01). Conclusions: Clodronate-containing liposomes protected against renal injury in SAP rats, and SPIO can be used as a tracer for MRI examination to detect renal injury in SAP rats. SPIO-aided MRI provided an efficient non-invasive way to monitor the migration of macrophages after renal injury in rats with SAP.

Key words: Pancreatitis, Clodronate disodium, Macrophage, Kidney injury
doi:10.1631/jzus.B1300244 **Document code:** A **CLC number:** R657.5$^+$1

1 Introduction

Severe acute pancreatitis (SAP) can cause systemic inflammatory response syndrome (SIRS) and high morbidity. Recently, the SIRS has been widely recognized as a disease state, which could lead to multiple organ failure (MOF) (Singh *et al*., 2009; Fry, 2012). SAP is often complicated by renal injury. The acute kidney injury is a serious complication of SAP and has a high mortality rate (Zhang *et al*., 2008; Li *et al*., 2010). It is not clear how renal injury is induced in acute pancreatitis but increasing evidence implicates pro-inflammatory cytokines and oxidative stress in the development of systemic complications.

‡ Corresponding author

* Project supported by the National Natural Science Foundation of China (No. 81070287) and the Natural Science Foundation of Jiangsu Province (Nos. BK2011484 and 2012704), China

It was suggested that impaired clearance of injured acini by macrophages is associated with an altered cytokine reaction resulting in the progression of acute pancreatitis. Macrophages play a central role in the systemic generation of inflammation mediators during acute pancreatitis (Shrivastava and Bhatia, 2010). Their accumulation and activation in the kidney were correlated with the progression of SAP and participated in the initiation, progression, and final destruction of renal tissue (Ricardo *et al*., 2008).

Clodronate is a first-generation bisphosphonate osteoporosis drug that is a potent osteoclast inhibitor, and has poor cellular membrane permeability and a short half-life in the systemic circulation (van Rooijen and Sanders, 1994; Selander *et al.*, 1996; Danenberg *et al.*, 2002; Hoshino and Yamazaki, 2005; Roelofs *et al.*, 2006). Clodronate-liposome selectively depleted macrophages from tissue by competing with ATP (van Rooijen and Sanders, 1994). When administered intravenously, liposomes are delivered to phagocytic cells of the mononuclear phagocyte system, and clodronate is released intracellularly, which destroys these phagocytic cells (Pennanen *et al.*, 1995; Day *et al.*, 2005; Jo *et al.*, 2006).

Due to their ability to produce proinflammatory cytokines, macrophages have long been regarded as classic mediators of innate immunity, glomerular damage, tubular cell death, and the downstream fibrotic events leading to renal injury (Bonventre and Zuk, 2004; Devarajan, 2006). Although it has been reported that adenosine triphosphate (ATP) depletion, reactive oxygen species (ROS), phospholipase activation, neutrophil infiltration, and vasoactive peptides were involved in the pathogenesis of renal damage (Williams *et al*., 2010; Zheng *et al*., 2011), the mechanisms underlying the macrophage-mediated renal injury have not been fully understood.

There was an attempt to determine the relationship between the involvement of renal and perirenal space and the severity of acute pancreatitis with magnetic resonance imaging (MRI) (Li *et al*., 2012). Superparamagnetic iron oxide (SPIO) nanoparticles have been used as cell labeling agent in both preclinical and clinical settings. The aim of this study was to evaluate the ability of macrophage imaging with SPIO-enhanced MRI to detect the infiltration of macrophages into pancreas and kidney to elucidate the role of macrophages in SAP-induced renal injury.

2 Materials and methods

2.1 Reagents

Clodronate (clodronic acid) was purchased from the Wegene Technoloies Inc. (Shanghai, China). Ferric hexahydrate, absolute ethanol, and cyclohexane (analytical reagent), oleic acid (OA), and $Fe(acac)_3$ (chemical pure) were purchased from Sinopharm Chemical Reagent Co. Ltd. (China). Apoptosis was detected by terminal deoxynucleotidyl transferase dUTP nick end labeling (TUNEL) assay with a detection kit (Cat. No. 11684817910; Roche, Switzerland). The CD68 immunohistochemical kit was purchased from the Fuzhou Maxim Biosciences (China), and tumor necrosis factor-α (TNF-α) was purchased from Invitrogen Corp. (California, USA). All other chemicals, unless otherwise stated, were purchased from Sigma (St. Louis, MO, USA). Electric stirrer (JJ-1) was purchased from the Jintan Medical Instrument Factory (Jiangsu, China), automatic biochemistry analyzer from Shimadzu (Japan), rotary evaporators R-200 from BUCHI, and MR (3.0 T), Bruker D500 Theta/2Theta X-Ray Diffraction (XRD) from SIEMENS. Transmission electron microscopes (TEM; FEI Tecnai-12) were obtained from Philips (the Netherlands).

2.2 Preparation of SPIO, SPIO-liposomes, and SPIO-clodronate-liposomes

Superparamagnetic Fe_3O_4 nanoparticles were prepared by chemical coprecipitation method as previously described (Zhang *et al.*, 2010). The black precipitate was obtained and washed with anhydrous alcohol thrice. Then the product was dispersed in anhydrous alcohol. The surface structure and morphology of the composite were characterized by XRD using Cu Kα radiation (λ=1.54 Å), scanning electron microscope (SEM), and TEM (voltage 120 kV). SPIO-liposomes (empty liposomes) and SPIO-clodronate-liposomes were prepared as the method previously described with some modifications (van Rooijen and van Kesteren-Hendrikx, 2003; Zhang *et al.*, 2010). Briefly, 0.14 g lecithin and 0.028 g cholesterol were dissolved in 15 ml chloroform. The mixture was then evaporated to remove chloroform by rotary distillation with 150 r/min at 37 °C. Finally, a layer of single-molecule lipid membrane was formed on the flask walls. The flask was dried in a 60 °C thermostatic

oven. Disodium clodronate (0.1 g) and prepared SPIO (2 drops) were added into 15 ml of phosphate buffered saline (PBS), vigorous shaking followed by 1 h continuous ultrasound to generate a phospholipid bilayer from the single-molecule phospholipid membranes. The resulting liposomes were washed with saline and PBS to remove unincorporated phospholipid molecules. Drug encapsulation efficiency was calculated as (liposome encapsulated drug/total liposomes)×100%. Calculated drug encapsulation efficiency of prepared clodronate-SPIO liposomes was 26.3%.

2.3 Animal models and experimental grouping

Sprague-Dawley rats (weight 350–400 g) were maintained in a temperature-controlled environment with an ambient temperature of 21–23 °C and a 12-h light/dark cycle. The rats were given food and water *ad libitum* and fasted overnight before experiments. Rat SAP models were prepared by the method of Zhang *et al.* (2007). The SAP rats were slowly injected 2 ml/kg body weight through the tail vein of either SPIO-liposomes (P group), SPIO-clodronate-liposomes (T group), or saline (C group). There were eight rats in each group. All dosages had previously been shown to be effective (Chamberlain *et al.*, 2011). The suspension was shaken gently before administration. Rat kidneys were scanned by T2-weighted MRI scans (in the same plane). Following the SAP model for 2 and 6 h, rats were sacrificed and the left kidney and pancreas were harvested. All institutional and national guidelines for the care and use of laboratory animals were followed.

2.4 Analyses of serum amylase (SAM), blood urea nitrogen (BUN), serum creatinine (SCr), and tumor necrosis factor-α (TNF-α) levels

At the end of the scans, 2 ml of blood samples were drawn from the superior mesenteric vein and placed on ice for 15 min before being centrifuged at 3000 r/min for 5 min, and kept at −70 °C until the analyses for SAM, BUN, SCr, and TNF-α. SAM, BUN, and SCr were measured by an automated enzymatic method (Shimadzu, Japan). Serum TNF-α was measured by enzyme-linked immunosorbent assays (ELISA) (Invitrogen, USA) according to the manufacturer's protocol.

2.5 MRI scan of kidney

MRI was performed using a 3.0 MRI system (Magnetom Trio Tim, SIEMENS). The MR images were acquired using a T2-weighted image scan with the parameters as Zhang *et al.* (2010) reported. A breast coil, self-made fixation tool for rats, water model, and image post-processing workstation (Leonardo) were utilized. The rats were put through the center of the coil along the vertical direction (that is, the long axes of the rat and the coil were mutually perpendicular). Physiological saline solution was placed below the coil for MRI. All rats were placed in the supine position. After rats were fixed using the self-made fixation tool, they were wrapped through the coil and put on the scanning bed. The MR images were acquired using coronal SE-T2WI (T2-weighted image) scans.

2.6 Perls Prussian blue staining

Perls Prussian blue staining of formalin-fixed, paraffin-embedded renal tissue sections (5 μm thick) used the method described by Tseng *et al.* (2009).

2.7 TUNEL assay

Tissue apoptotic cells were detected with TUNEL using a commercial kit (No. 11684817910; Roche, Switzerland) according to the manufacturer's protocol. TUNEL assay was performed for paraffin sections fixed with 4% paraformaldehyde and processed according to the method previously described by Kitamoto *et al.* (2009).

2.8 Immunohistochemistry staining of renal macrophages

Kidney infiltrating macrophages were evaluated by immunostaining of $CD68^+$ as described previously (Dang *et al.*, 2010). Briefly, formalin-fixed, paraffin-embedded tissue sections (4 μm) were blocked with 10% normal rabbit serum in Tris-buffered saline for 20 min followed by 15 min incubation with avidin and then biotin using an avidin-biotin blocking kit (Vector Laboratories). Endogenous peroxidase activity was inhibited by 20-min incubation with methanol containing 0.3% H_2O_2. Sections were incubated with a monoclonal antibody (mAb) against rat $CD68^+$ for 12 h at 4 °C, and then incubated with biotin-labeled

goat anti-mouse IgG for 30 min followed by a 30-min incubation with avidin at room temperature. Biotinylated horseradish peroxidase was applied for 30 min. Slides were washed with Tris-buffered saline with Tween 20 (TBST) thrice after each incubation. Peroxidase activity was developed in 3,3-diaminobenzidine and counterstained with Mayer's hematoxylin.

2.9 Histological examination

Paraffin-embedded pancreas and kidneys were sectioned (5 μm), then stained with hematoxylin and eosin (H&E). Experienced histologists checked and scored each specimen blindly. This pathological assessment of pancreatic tissue was performed according to the scoring criteria proposed by Kaiser *et al.* (1995). Histopathologic analysis of the renal injury was performed according to the previously described scoring system (Zhang *et al.*, 2006): 0: normal finding; I: no cellular proliferation or fibrosis in renal glomerulus, no capillary congestion or microthrombus, swelling and blurry boundary of renal tubular epithelial cell, stegnosis or atresia of lumens, protein cast and renal interstitial edema; II: glomerular capillary congestion, scattered necrosis in renal tubular epithelial cell, interstitial edema, and inflammatory cell infiltration; III: all the indications in II plus lamellar necrosis of renal tubular epithelial cell.

2.10 Statistical analysis

All the data were expressed as mean±standard deviation (SD) and analyzed with SPSS statistical software (18.0). If equal variances were assumed, one-way analysis of variance (ANOVA) was employed; otherwise, the Kruskal-Wallis test was used. A P value <0.05 was considered statistically significant.

3 Results

3.1 Characterization of SPIO and liposomes

SPIO nanoparticles were aggregated together with an average diameter of approximately 20–50 nm, which is consistent with TEM results. The homemade SPIO colloid solution exhibited nanometer particle diameter, excellent stability, and magnetic response, and was superparamagnetic. Transmission electron micrographs measurements revealed that SPIO-liposomes were spherical with a uniform size around 100–200 nm in diameter (Fig. 1).

3.2 Changes in the levels of SAM, BUN, SCr, and TNF-α

Levels of SAM, BUN, SCr, and TNF-α of the P group rats were significantly higher than those of the C group rats at each time point (P<0.01), while they

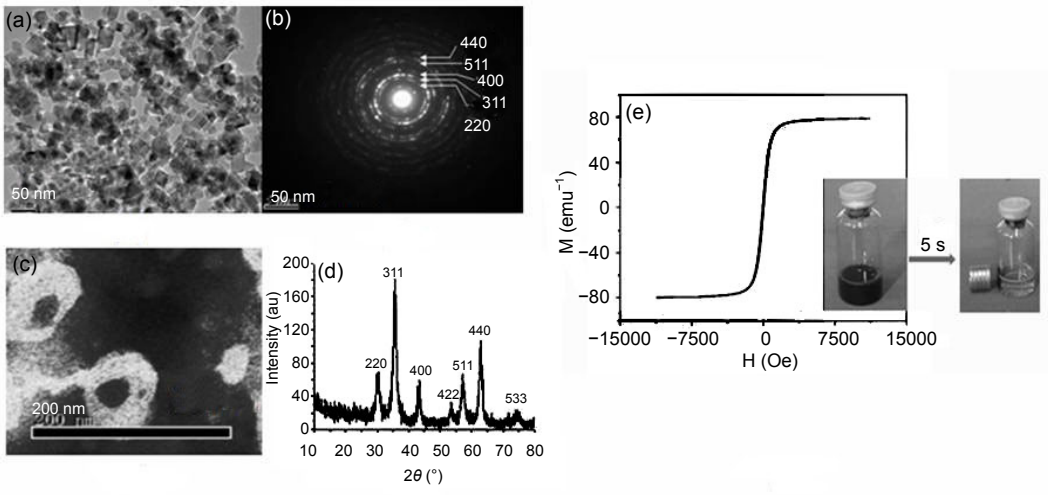

Fig. 1 Characterization of SPIO and liposomes

(a, b) Morphology and size of the particles were measured by SEM and TEM, respectively; (c) SPIO-clodronate-containing liposomes were similar in size, and iron particles were distributed uniformly (Zhang *et al*., 2010); (d) XRD spectrum of Fe_3O_4 shows the typical pattern whose peaks can be indexed to the standard XRD pattern of Fe_3O_4 (JCPDS: 19-0627); (e) Hysteresis loop of the Fe_3O_4 nanoparticles at 300 K and insets show the digital images of the resultant Fe_3O_4 sample, which was magnetically harvested in 5 s

were markedly decreased in the T group rats compared to those in the P group rats at all time points (P<0.01; Fig. 2).

3.3 Pathological changes in the pancreas

Pancreases of the C group rats did not show significant changes. In the opened abdominal cavity of rats, an amount of bloody ascites was obvious in the P group rats. At different time points, we could see different degrees of edema, hemorrhage, and necrosis of the pancreas in the P group. The pancreatic pathological changes in the T group were significantly reduced compared with those in the P group. Pancreatic histological scores of the P and T groups were significantly higher than that of the C group. Our results revealed that there was a significant and dramatic histological improvement in the T group compared to the P group (P<0.01; Fig. 3).

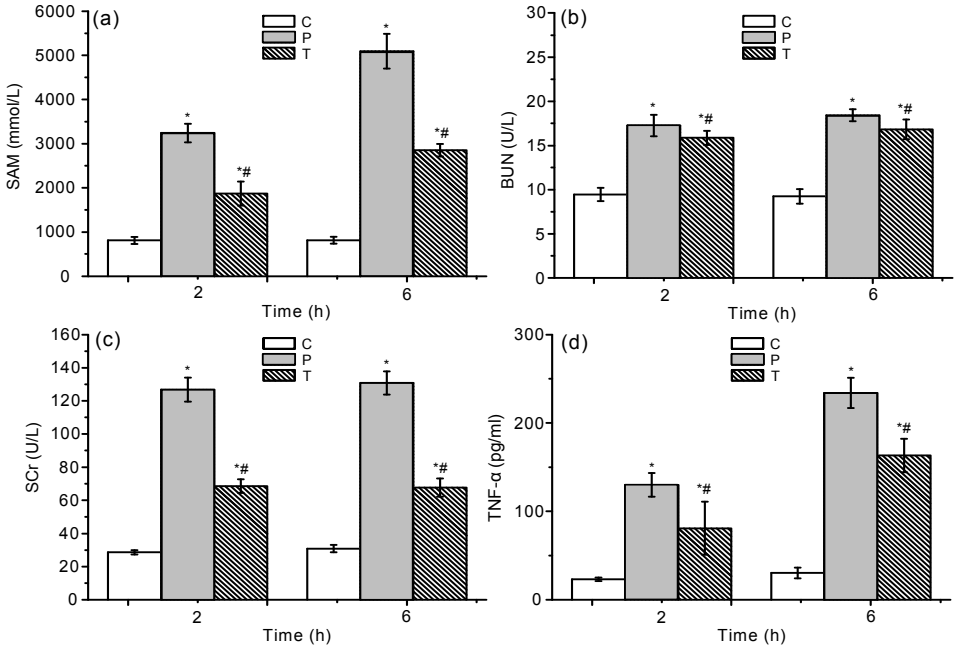

Fig. 2 Levels of SAM (a), BUN (b), SCr (c), and TNF-α (d) in the three groups at 2 and 6 h

The figures of (a) and (d) are from Zhang *et al*. (2010). * P<0.01, vs. the C group; # P<0.01, vs. the P group. Data are expressed as mean±SD (n=8)

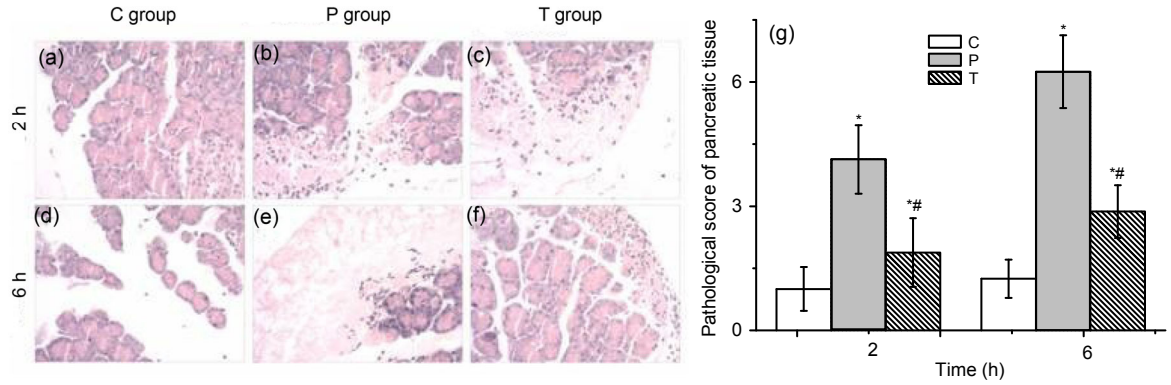

Fig. 3 Pathological changes in the pancreas

(a, d) In the C group, the pancreata of rats showed no morphological or structural abnormalities. (b, e) In the P group, there were varying degrees of focal interlobular edema, necrotic areas without structure, and red blood cells in the tissue space, as well as massive inflammatory cell infiltration. (c, f) In the T group, pancreatic edema, hemorrhage, and necrosis, as well as inflammatory cell infiltration were milder than those in the P group. Magnification is 200×. (g) Pancreatic histological scores showed significant differences between the P and T groups and the C group (* P<0.01); pathological changes in the T group were less severe than those in the P group (# P<0.01) (Zhang *et al*., 2010). Data are expressed as mean±SD (n=8) (Note: for interpretation of the references to color in this figure legend, the reader is referred to the web version of this article)

3.4 Gross changes and light microscopic changes of kidney

The kidneys of the C group rats showed normal morphology without swelling and bleeding points. Varying degrees of congestion and swelling were seen in the P group rats at all time points, the kidney became darker in color, and scattered necrotic foci were visible. In the T group, the above-mentioned changes were milder than those in the P group at all time points.

The kidneys of the C group rats showed no obvious renal morphological or structural abnormalities in most rats. In the P group, there were capillary congestion of renal glomerulus, swelling, scattered necrotic foci, and blurry boundary of the renal tubule epithelial cell, stenosis or atresia of lumens, visible protein cast, interstitial edema and inflammatory cell infiltration at 2 h, interstitial edema and inflammatory cell infiltration at 6 h. The floss and red cell with eosinophilic staining were found in the renal glomerulus and homogenous or red cell cast with eosinophilic staining in the renal tubule. There was necrosis of the lamellar epithelial cell in a few rats. The T group rats had those changes to a milder degree. Renal histological scores showed significant differences between the P and T groups and the C group; pathological changes in the T group were less severe than those in the P group (Fig. 4).

3.5 Changes in MRI T2-weighted image

The kidney MRI T2-weighted image signal intensity of the P and T group rats was significantly lower than that of the C group rats at 2 and 6 h (Fig. 5).

3.6 Perls Prussian blue staining

The Prussian blue staining did not have any positive staining in renal tissues of the C group rats but showed numerous blue stained cells in the kidney of the P group rats and the number of stain-positive kidney cells was greatly diminished in the T group rats (Fig. 6).

3.7 Immunohistochemistry for macrophage markers (CD68) in renal tissue

Macrophage infiltration of renal tissue was assessed by immunostaining for the macrophage-specific marker CD68. Clusters of CD68-positive cells with structural damages were seen in the kidney of the P group rats while fewer CD68-positive cells were detected in the T group rat kidney (Fig. 7).

3.8 Ratio of apoptosis of renal tissues by TUNEL

Large numbers of TUNEL-positive cells were observed in the T group, but no or minimal TUNEL-positive cells were observed in the C and P groups (Fig. 8).

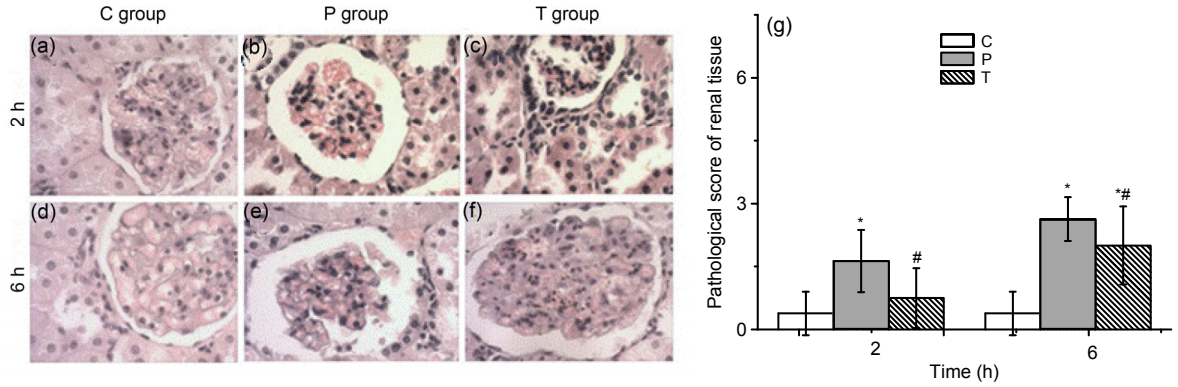

Fig. 4 Pathological changes and histological scores in the kidney

(a, d) The C group showed no obvious abnormality. (b, e) In the P group, basically no abnormal changes were shown in 2 h tubular epithelial cell structure, glomerular structure was slightly fuzzy, and interstitial boundaries were unclear; 6 h tubular high degree of swelling of the epithelial cells was shown. The epithelial cells showed varying degrees of necrosis, renal tubular red tube, some of the specimens in protein casts, fuzzy glomerular structure, and ill-defined interstitium, and a large number of red blood cells were aggregated. (c, f) In the T group, tubular epithelial degeneration, compared with the P group, improved markedly. Magnification is 200×. (g) Renal histological scores showed significant differences between the P and T groups and the C group ($^{*}P<0.01$); pathological changes in the T group were less severe than those in the P group ($^{\#}P<0.01$). Data are expressed as mean±SD (n=8) (Note: for interpretation of the references to color in this figure legend, the reader is referred to the web version of this article)

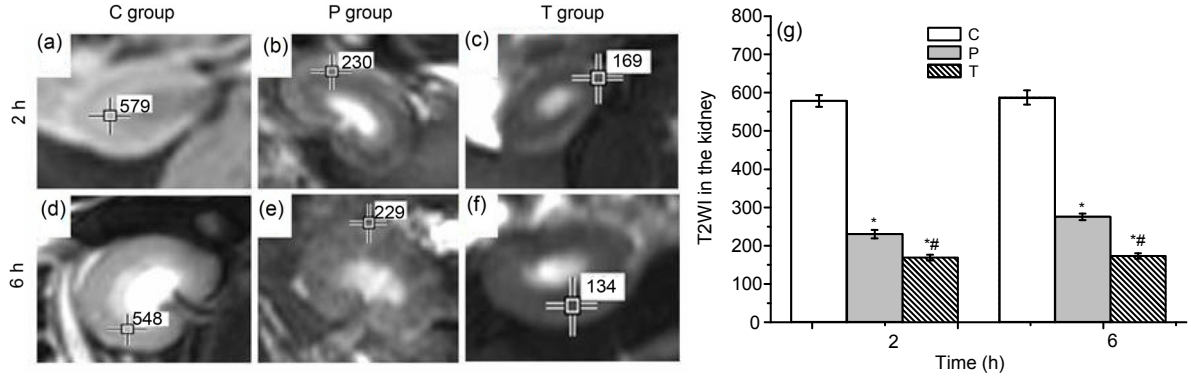

Fig. 5 Signal intensity of the kidney on T2-weighted image (T2WI) in the C (a, d), P (b, e), and T (c, f) groups and significantly lower signal intensity in the P and T groups than that in the C group (g)

$^{*}P<0.01$, vs. the C group; $^{\#}P<0.01$, vs. the P group. Data are expressed as mean±SD (n=8)

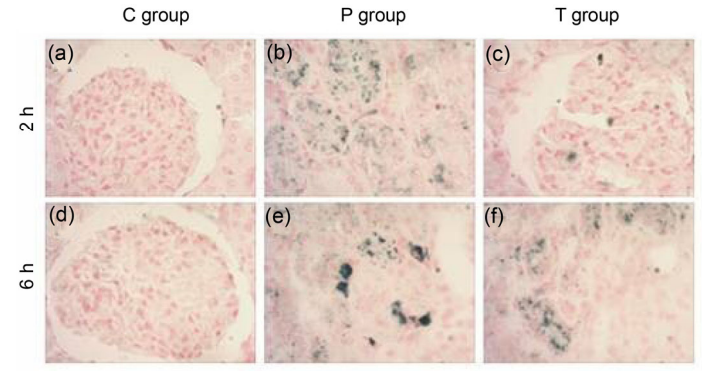

Fig. 6 Perls Prussian blue staining in renal tissues

(a, d) Perls Prussian blue staining showed that no extracellular iron deposits were observed in the C group at 2 and 6 h; (b, e) Numerous blue iron-positive cells are located in the glomerulus, which reflects intense SPIO uptake by renal macrophages in the P group at 2 and 6 h; (c, f) Poor staining reflects the presence of only a few iron-loaded renal macrophages in the T group. Magnification is 200× (Note: for interpretation of the references to color in this figure legend, the reader is referred to the web version of this article)

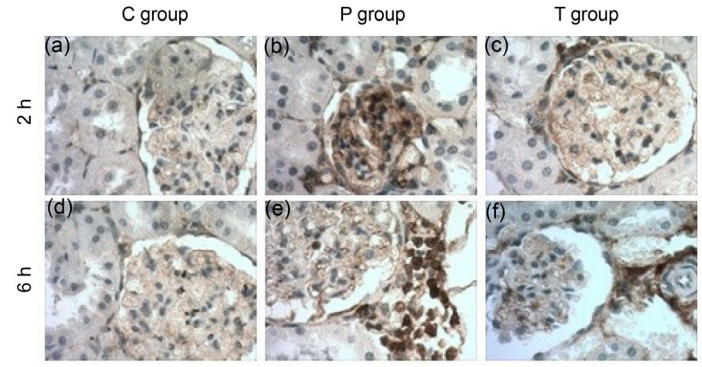

Fig. 7 Immunohistochemical staining for CD68 in rat kidney tissue sections

(a, d) CD68-positive cells were seldom seen in the control rats; (b, e) Numerous CD68-positive cells clusters were observed in the P group rat kidney with tissue architecture being massively disrupted; (c, f) Fewer CD68-positive cells were observed in kidney tissue sections from the T group. Magnification is 200×

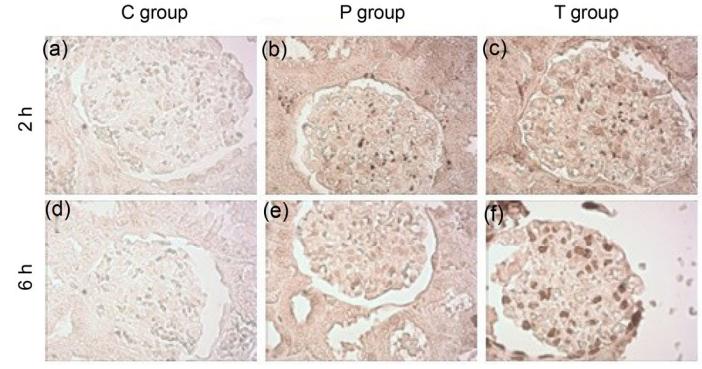

Fig. 8 TUNEL *in situ* detection of apoptosis

The apoptosis of kidney cells in the C (a, d), P (b, e), and T (c, f) group rats was assessed by TUNEL assay at 2 and 6 h. Magnification is 200×

4 Discussion

SAP is a complex inflammatory syndrome which could cause high mortality. The morbidity and incidence of serious complications of SAP remain high due to the lack of efficient treatment. SAP is often complicated by acute kidney injury, either isolated or part of MOF (Peride *et al.*, 2011). Patients with SAP complicated with acute kidney injury are associated with a higher mortality than patients with acute pancreatitis alone (Lin *et al.*, 2011; Bishehsari *et al.*, 2012). Multiple studies have demonstrated that sepsis is the leading cause of acute renal failure among risk factors like polytrauma, burns, pancreatitis, cardiopulmonary bypass, and others. During acute pancreatitis, especially SAP, massive pro-inflammatory cytokines are released from pancreatic tissues, which in turn influence the whole process of pancreatitis.

Macrophage infiltration in the kidney, especially in the tubulointerstitium, is closely related to renal tissue damage (such as interstitial fibrosis and crescent formation), proteinuria, and nephritic dysfunction. Kidney injuries usually have visible renal macrophage infiltration. Macrophage infiltration is not only a secondary response to injury, but also is actively involved throughout the process of kidney injury. Thus, targeting selected macrophage pathways is a potential therapeutic strategy for suppressing macrophage-mediated renal injury.

SPIO is a new type of magnetic material used in MRI, which can be developed as a reticuloendothelial system. MRI contrasts agents with markedly shortened T2 and moderately affected T1 relaxation rates (Bulte and Kraitchman, 2004). Intravenously administrated SPIO particles can be specifically taken up by macrophages (Siglienti *et al.*, 2006; Hauger *et al.*, 2007; Bierry *et al.*, 2008; 2009). The signal intensity of T2-weighted image of kidney decreased more significantly in the P group than in the C group. As a non-specific extracellular contrast material, SPIO has been widely used in MRI of parenchymatous organs. Dynamic SPIO-enhanced MRI can provide useful information about the blood supply to lesions and thus greatly improve the accuracy of diagnosis of focal renal lesions. MRI detection of macrophages homing to an injured kidney may facilitate early detection and investigation of the pathogenesis of acute kidney injury and be a strategy for determining the treatment of acute renal failure (Cai *et al.*, 2012).

Macrophages are key pro-inflammatory and anti-inflammatory cells, which accumulate in the damaged organ in SAP. By using the property of SPIO, SAP complicated by multiple organ injury can use noninvasive molecular MRI for evaluation. We employed liposomes as carriers to deliver clodronate into macrophages to induce apoptosis, reduce the release of inflammatory mediators, and deliver SPIO for MRI examination of renal injury. In our model, we used immunohistochemistry to study the expression of CD68 in the kidney of SAP rats at different time points. We can find that CD68 expression in renal tissue increased significantly in the P group. SAM and TNF-α levels increased more significantly in the P group than in the C group, and were significantly lower in the T group than in the P group. Coincidentally, pancreas and renal injuries in the T group were milder than those in the P group.

In conclusion, clodronate-liposomes could prevent the progression of SAP-caused renal injury by modulating the inflammation process. We found a new method for making SPIO-liposomes to label the macrophage and MRI. The results may provide insights and new possibilities for the MRI evaluation and treatment of renal injury with SAP.

Acknowledgements

The authors thank Drs. Li-rong DUAN and De-li JIANG of Jiangsu University, China, for excellent technical assistance.

Compliance with ethics guidelines

Sheng-chun DANG, Yan-hua ZENG, Ping-jiang WANG, Bao-ding CHEN, Rong-fang CHEN, Arun KUMAR SINGH, Pankaj KUMAR, Shu FENG, Lei CUI, Hao WANG, and Jian-xin ZHANG declare that they have no conflict of interest.

All institutional and national guidelines for the care and use of laboratory animals were followed.

References

Bierry, G., Jehl, F., Boehm, N., *et al*., 2008. Macrophage activity in infected areas of an experimental vertebral osteomyelitis model: uspio-enhanced MR imaging—feasibility study. *Radiology*, **248**(1):114-123. [doi:10.1148/radiol.2481071260]

Bierry, G., Jehl, F., Boehm, N., *et al*., 2009. Macrophage imaging by uspio-enhanced MR for the differentiation of infectious osteomyelitis and aseptic vertebral inflammation. *Eur. Radiol*., **19**(7):1604-1611. [doi:10.1007/s00330-009-1319-4]

Bishehsari, F., Sharma, A., Stello, K., *et al*., 2012. TNF-α gene (*TNFA*) variants increase risk for multi-organ dysfunction

syndrome (MODS) in acute pancreatitis. *Pancreatology*, **12**(2):113-118. [doi:10.1016/j.pan.2012.02.014]

Bonventre, J.V., Zuk, A., 2004. Ischemic acute renal failure: an inflammatory disease? *Kidney Int*., **66**(2):480-485. [doi:10.1111/j.1523-1755.2004.761_2.x]

Bulte, J.W., Kraitchman, D.L., 2004. Iron oxide MR contrast agents for molecular and cellular imaging. *NMR Biomed*., **17**(7):484-499. [doi:10.1002/nbm.924]

Cai, Q.Y., Lee, H., Kim, E.J., *et al*., 2012. Magnetic resonance imaging of superparamagnetic iron oxide-labeled macrophage infiltrates in acute-phase renal ischemia-reperfusion mouse model. *Nanomedicine*, **8**(3):365-373. [doi:10.1016/j.nano.2011.06.019]

Chamberlain, C.S., Leiferman, E.M., Frisch, K.E., *et al*., 2011. The influence of macrophage depletion on ligament healing. *Connect. Tissue Res*., **52**(3):203-211. [doi:10.3109/03008207.2010.511355]

Danenberg, H.D., Fishbein, I., Gao, J., *et al*., 2002. Macrophage depletion by clodronate-containing liposomes reduces neointimal formation after balloon injury in rats and rabbits. *Circulation*, **106**(5):599-605. [doi:10.1161/01.CIR.0000023532.98469.48]

Dang, S.C., Jiang, D.L., Chen, M., *et al*., 2010. Clodronate-containing liposomes attenuate lung injury in rats with severe acute pancreatitis. *J. Zhejiang Univ.-Sci. B (Biomed. & Biotechnol.)*, **11**(11):828-835. [doi:10.1631/jzus.B1000044]

Day, Y.J., Huang, L., Ye, H., *et al*., 2005. Renal ischemia-reperfusion injury and adenosine 2A receptor-mediated tissue protection: role of macrophages. *Am. J. Physiol. Renal Physiol*., **288**(4):F722-F731. [doi:10.1152/ajprenal.00378.2004]

Devarajan, P., 2006. Update on mechanisms of ischemic acute kidney injury. *J. Am. Soc. Nephrol*., **17**(6):1503-1520. [doi:10.1681/ASN.2006010017]

Fry, D.E., 2012. Sepsis, systemic inflammatory response, and multiple organ dysfunction: the mystery continues. *Am. Surg*., **78**(1):1-8.

Hauger, O., Grenier, N., Deminere, C., *et al*., 2007. Uspio-enhanced MR imaging of macrophage infiltration in native and transplanted kidneys: initial results in humans. *Eur. Radiol*., **17**(11):2898-2907. [doi:10.1007/s00330-007-0660-8]

Hoshino, H., Yamazaki, K., 2005. Mechanisms of action in bisphosphonates. *Clin. Calcium*., **15**(7):88-92.

Jo, S.K., Sung, S.A., Cho, W.Y., *et al*., 2006. Macrophages contribute to the initiation of ischaemic acute renal failure in rats. *Nephrol. Dial. Transplant.*, **21**(5):1231-1239. [doi:10.1093/ndt/gfk047]

Kaiser, A.M., Saluja, A.K., Sengupta, A., *et al*., 1995. Relationship between severity, necrosis, and apoptosis in five models of experimental acute pancreatitis. *Am. J. Physiol*., **269**(5 Pt 1):C1295-C1304.

Kitamoto, K., Machida, Y., Uchida, J., *et al*., 2009. Effects of liposome clodronate on renal leukocyte populations and renal fibrosis in murine obstructive nephropathy. *J. Pharmacol. Sci*., **111**(3):285-292. [doi:10.1254/jphs.09227FP]

Li, H., Qian, Z., Liu, Z., *et al*., 2010. Risk factors and outcome of acute renal failure in patients with severe acute pancreatitis. *J. Crit. Care*, **25**(2):225-229. [doi:10.1016/j.jcrc.2009.07.009]

Li, X.H., Zhang, X.M., Ji, Y.F., *et al*., 2012. Renal and perirenal space involvement in acute pancreatitis: an MRI study. *Eur. J. Radiol*., **81**(8):e880-e887. [doi:10.1016/j.ejrad.2012.04.032]

Lin, H.Y., Lai, J.I., Lai, Y.C., *et al*., 2011. Acute renal failure in severe pancreatitis: a population-based study. *Ups. J. Med. Sci*., **116**(2):155-159. [doi:10.3109/03009734.2010.547636]

Pennanen, N., Lapinjoki, S., Urtti, A., *et al*., 1995. Effect of liposomal and free bisphosphonates on the IL-1β, IL-6 and TNFα secretion from raw 264 cells *in vitro*. *Pharm. Res*., **12**(6):916-922. [doi:10.1023/A:1016281608773]

Peride, I., Checherită, I.A., Ciocâlteu, A., *et al*., 2011. Acute-on-chronic renal disease caused by pancreatitis—impact of renal replacement therapy. *Chirurgia (Bucur)*, **106**(1):83-89 (in Romanian).

Ricardo, S.D., van Goor, H., Eddy, A.A., 2008. Macrophage diversity in renal injury and repair. *J. Clin. Invest*., **118**(11):3522-3530. [doi:10.1172/JCI36150]

Roelofs, A.J., Thompson, K., Gordon, S., *et al*., 2006. Molecular mechanisms of action of bisphosphonates: current status. *Clin. Cancer Res*., **12**(20 Pt 2):6222s-6230s. [doi:10.1158/1078-0432.CCR-06-0843]

Selander, K.S., Monkkonen, J., Karhukorpi, E.K., *et al*., 1996. Characteristics of clodronate-induced apoptosis in osteoclasts and macrophages. *Mol. Pharmacol*., **50**(5):1127-1138.

Shrivastava, P., Bhatia, M., 2010. Essential role of monocytes and macrophages in the progression of acute pancreatitis. *World J. Gastroenterol*., **16**(32):3995-4002. [doi:10.3748/wjg.v16.i32.3995]

Siglienti, I., Bendszus, M., Kleinschnitz, C., *et al*., 2006. Cytokine profile of iron-laden macrophages: implications for cellular magnetic resonance imaging. *J. Neuroimmunol.*, **173**(1-2):166-173. [doi:10.1016/j.jneuroim.2005.11.011]

Singh, V.K., Wu, B.U., Bollen, T.L., *et al*., 2009. Early systemic inflammatory response syndrome is associated with severe acute pancreatitis. *Clin. Gastroenterol. Hepatol*., **7**(11):1247-1251. [doi:10.1016/j.cgh.2009.08.012]

Tseng, H.H., Chang, J.G., Hwang, Y.H., *et al*., 2009. Expression of hepcidin and other iron-regulatory genes in human hepatocellular carcinoma and its clinical implications. *J. Cancer Res. Clin. Oncol*., **135**(10):1413-1420. [doi:10.1007/s00432-009-0585-5]

van Rooijen, N., Sanders, A., 1994. Liposome mediated depletion of macrophages: mechanism of action, preparation of liposomes and applications. *J. Immunol. Methods*, **174**(1-2):83-93. [doi:10.1016/0022-1759(94)90012-4]

van Rooijen, N., van Kesteren-Hendrikx, E., 2003. "*In vivo*" depletion of macrophages by liposome-mediated "suicide". *Methods Enzymol.*, **373**:3-16. [doi:10.1016/S0076-6879(03)73001-8]

Williams, T.M., Little, M.H., Ricardo, S.D., 2010. Macrophages in renal development, injury, and repair. *Semin. Nephrol.*, **30**(3):255-267. [doi:10.1016/j.semnephrol.2010.03.011]

Zhang, J.X., Dang, S.C., Qu, J.G., *et al*., 2006. Ligustrazine alleviates acute renal injury in a rat model of acute necrotizing pancreatitis. *World J. Gastroenterol.*, **12**(47):7705-7709.

Zhang, J.X., Dang, S.C., Zhang, Y., *et al*., 2010. MRI shows clodronate-liposomes attenuating liver injury in rats with severe acute pancreatitis. *Hepatobiliary Pancreat. Dis. Int.*, **9**(2):192-200.

Zhang, X.P., Zhang, L., He, J.X., *et al*., 2007. Experimental study of therapeutic efficacy of baicalin in rats with severe acute pancreatitis. *World J. Gastroenterol.*, **13**(5):717-724.

Zhang, X.P., Wang, L., Zhou, Y.F., 2008. The pathogenic mechanism of severe acute pancreatitis complicated with renal injury: a review of current knowledge. *Dig. Dis. Sci.*, **53**(2):297-306. [doi:10.1007/s10620-007-9866-5]

Zheng, D., Wang, Y., Cao, Q., *et al*., 2011. Transfused macrophages ameliorate pancreatic and renal injury in murine diabetes mellitus. *Nephron. Exp. Nephrol.*, **118**(4):e87-e99. [doi:10.1159/000321034]

中文概要：

本文题目：氯屈膦酸二钠-超顺磁性氧化铁脂质体减轻重症急性胰腺炎肾损伤

Clodronate-superparamagnetic iron oxide-containing liposomes attenuate renal injury in rats with severe acute pancreatitis

研究目的：探讨氯屈膦酸二钠-超顺磁性氧化铁（SPIO）脂质体对重症急性胰腺炎（SAP）肾损伤的保护作用。

创新要点：围绕 SAP 并发多器官损伤这一核心问题，联系巨噬细胞在 SAP 发病过程中的作用，使用纳米脂质体携带氯屈膦酸二钠及 SPIO，以及利用自体巨噬细胞对 SAP 时多器官损伤的定性靶向性以及磁性纳米颗粒的超顺磁性，应用磁共振成像（MRI）对 SAP 并发多器官损伤进行早期诊断。结合使用氯屈膦酸二钠，使其促进巨噬细胞的凋亡，减少其在急性胰腺炎早期产生炎症介质，阻止全身性炎症反应的进程，从而实现对多器官损伤的保护作用。

研究方法：采用胰腺被膜下均匀注射 5%牛磺胆酸钠制作 SAP 模型。SD 大鼠 48 只，随机分为对照组（C 组）、空白 SPIO 脂质体组（P 组）和氯屈膦酸二钠+SPIO 脂质体组（T 组）。P 组和 T 组大鼠制作 SAP 模型。制模 2 h 和 6 h 后取肠系膜上静脉血液，检测各组大鼠血清中淀粉酶、尿素氮、血肌酐和肿瘤坏死因子-α 的含量，观察胰腺及肾组织的病理学变化及进行病理评分，通过检测肾组织的 TUNEL 染色及 CD68 表达研究氯屈膦酸二钠-超顺磁性氧化铁脂质体对肾组织巨噬细胞凋亡的影响并进行 MRI 诊断。

重要结论：氯屈膦酸二钠-超顺磁性氧化铁脂质体可选择性清除单核/巨噬细胞，减少炎症介质释放，对 SAP 大鼠胰腺及肾损伤有保护作用。SPIO 可作为 MRI 示踪。

关键词组：氯屈膦酸二钠；超顺磁性氧化铁；巨噬细胞；重症急性胰腺炎；肾损伤